Multiphysics modeling and optimization of the driving strategy of a light duty fuel cell vehicle

Jean-Christophe Olivier, Guillaume Wasselynck, Stéphane Chevalier, Bruno Auvity, Christophe Josset, Didier Trichet, Gaetano Squadrito, Nicolas Bernard

Multiphysics modeling and optimization of the driving strategy of a light duty fuel cell vehicle

Jean-Christophe Olivier [a,*], *Guillaume Wasselynck* [a], *Stéphane Chevalier* [b], *Bruno Auvity* [c], *Christophe Josset* [c], *Didier Trichet* [a], *Gaetano Squadrito* [d], *Nicolas Bernard* [a]

[a] *Nantes University, IREENA Laboratory, Saint-Nazaire, France*
[b] *Thermofluids for Energy and Advanced Materials Laboratory, University of Toronto, Canada*
[c] *Nantes University, Laboratoire de Thermocinétique de Nantes, Nantes, France*
[d] *CNR-ITAE, Messina, Italy*

ARTICLE INFO

Article history:
Received 4 August 2016
Received in revised form
22 May 2017
Accepted 21 June 2017
Available online 21 August 2017

Keywords:
Fuel-cell powertrain
Multi-physics modeling
Optimization
Eco-marathon

ABSTRACT

This paper presents the optimization of the driving strategy of a high efficiency fuel cell based power train. This power train is developed to equip a light duty urban-concept vehicle that runs energetic races. The objective is to go the furthest with the lowest quantity of fuel. A comprehensive dynamical model is presented, including the mechanical requirement, the thermal behavior of the fuel cell stack and the various losses and consumptions of the power train devices. This model is next integrated into a global optimization algorithm, to determine the best race strategy to be adopted. These results are validated on experimental measurements, obtained during a real race at the Shell Eco-Marathon, in 2015.

Introduction

Given the new economic and ecological issues, car manufacturers should focus on alternative energy sources, such as electric batteries or fuel cells [8,10,27,32,33,35,36,38]. Although still young and hard to handle, fuel cells, and particularly Proton Exchange Membrane Fuel Cells (PEMFCs), remain a promising way. Indeed, a hydrogen fuel cell vehicle has naturally a better performance than a diesel car (usually 30% against 22% of efficiency at the wheel). Moreover, the energy supplied by the fuel cell is electric, which allows propulsion chains more flexible with high performances [11,37]. For several years, a prototype vehicle with extremely low energy consumption has been developed by researchers and electrical engineering students, to run energetic races [28,34,39]. The energy source of this vehicle is a PEMFC. From 2010 to 2012, this vehicle has been recognized by the Shell group (through the 2010 edition of the Shell Eco-marathon competition, on the EuroSpeedway race track, Germany) as the world most energy efficient car, with an equivalent consumption of only 0.02 L of unleaded gasoline 95 per 100 km, at a minimum average speed of 30 km/h.

Since 2013, a new car with extremely low energy consumption is developed (see Fig. 1). It comes under the urban-

* *Corresponding author.*
E-mail address: jean-christophe.olivier@univ-nantes.fr (J.-C. Olivier).

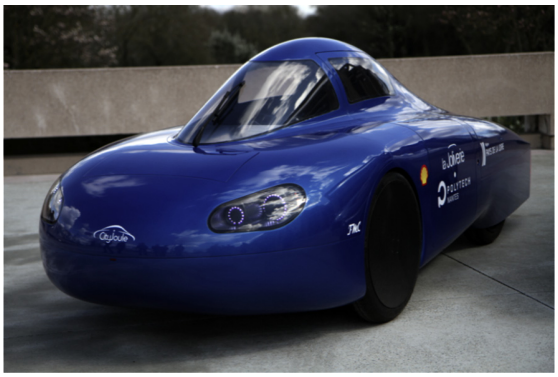

Fig. 1 – The Urban-Concept vehicle Cityjoule.

concept category, which aims to promote the development of vehicles closest to true city cars. The energy source of this vehicle is also a PEMFC. To achieve an energy consumption as low as possible, each element of the vehicle must be optimized, from the mechanical angle (drag coefficient, frontal area, slop, road-wheel friction, weight) to the electrical architecture (power converter, motor efficiencies and fuel cell peripheral elements consumption). This optimization has been done in previous works, but without taking into account the driving strategy [34]. In this paper, the optimal driving strategy that minimizes the car energy demand is presented. It is based on a multi-physics modeling of the power train, taking into account the road profile and the race constraints (average speed, stop at each turn, etc.) [1,5,7,31]. This model is then integrated into a global optimization algorithm, which lead to the best velocity profile, motor current and gearbox ratio.

The paper is structured as follows: In section Presentation of the race and vehicle characteristics, the vehicle specifications and the race characteristics are presented. A focus is made on power train architecture from the fuel cell stack to the mechanical needs. In section Multi-Physics modeling of the powertrain, a dynamical and multi-physics model is developed. In this section, each part of the power train is presented. An originality of this work is the addition of a thermal modeling of the PEMFC, in order to take into account the auxiliary stack consumption in energy balance, including the air feeding and cooling systems. The optimization results are given in Section Results, which allow to achieve a driving strategy minimizing the final energy consumed by the vehicle. Simulations and experimental results are compared to a real race, recorded during the previous edition of the Shell eco-marathon, in Rotterdam, Netherlands. Conclusions are given in Section Conclusions.

Presentation of the race and vehicle characteristics

The urban-concept car and its associated fuel cell power train were both designed and built to participate in the Shell Eco Marathon energetic race (Rotterdam, Netherlands). The principle of such a competition is to drive a vehicle with one pilot the furthest with the lowest quantity of fuel at a minimum average speed of 25 km/h. A minimum weight of 70 kg is imposed for the pilot. Each competitor will have to travel 10 laps of the race track corresponding to 16.1 km in less than 40 min. In the urban-concept category, a stop is mandatory during at each lap. To evaluate prototype car efficiency, the fuel quantity carried on board is measured before and after the attempt. Wide range of fuels can be used (Unleaded gasoline; diesel; LPG; GTL; fatty acid methyl ester; ethanol E100 and hydrogen). In the fuel cell category, an official flow meter is used to measure the volume of hydrogen consumed during the attempt. This amount of energy is converted into kilometers per kWh. It is important to notice that in the fuel cell category, battery is not allowed in the car except for safety purposes, i.e. to power the car-horn and the hydrogen sensor.

Multi-physics modeling of the powertrain

In this section, a dynamical model of the vehicle is proposed. For a set of input parameters (e.g. motor current, road slope, ambient temperature, …), this model calculates the evolution of the various system states, the losses and the consumption of each subsystem (see Fig. 2).

This model is organized around six main blocks: The mechanical part, the propulsion motor, the power converter, the fuel cell, the stack accessories coupled to a thermal model, and the control laws and supervision. This dynamical model is oriented towards the optimization and must be solved quickly. Thus, only the velocity v and the stack temperature T_{st}, which are the slowest state variables, are taken into account. All other dynamics are considered fast enough to be regarded as instantaneous (see Fig. 3).

The urban-concept *Cityjoule* presented in this paper is made of two identical power trains, each supplying one of the two rear wheels. In the next sections, only one power train is studied.

Fuel cell

The fuel-cell stack has a power rate of 800 W and is composed of 28 cells connected in series, each of them having an active area of 60 cm^2. A PEMFC is mainly described by its polarization curve. It gives the voltage level U_{st} according to the supplied current I_{st}. The electrochemical equations give a relation

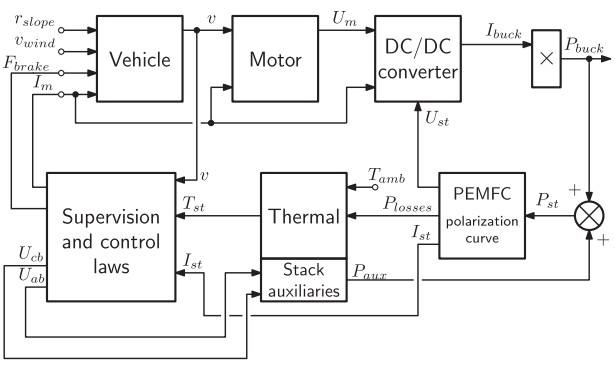

Fig. 2 – Tank-to-wheel model.

between the output voltage U_{st} (in V) and the stack efficiency η_{stack}:

$$\eta_{stack} = \frac{1000\, f\, U_{st}}{n_{cells}\, LHV_{H_2}} \tag{1}$$

where f is the Faraday constant (96,485.34 C mol^{-1}), n_{cells} the cells number and LHV_{H_2} the lower heating value of hydrogen (119.96 10^6 J kg^{-1}). Moreover, the hydrogen flow Q_{H2} (l/s), i.e. the instantaneous hydrogen consumption, is linked to the output current I_{st}:

$$Q_{H2} = \frac{I_{st}\, n_{cells}\, M_{H_2}}{f \rho_{H_2}} \tag{2}$$

where ρ_{H2} is the hydrogen density and M_{H2} is the molar mass of hydrogen.

Power converter

The proposed DC/DC power converter used in the power train is a classical asynchronous buck converter, located between the PEMFC and the DC-motor (see Fig. 3).

This model take into account the losses in the power stage (conduction and commutation losses of MOSFET and Schottky diode), in the smooth inductance (copper and magnetic losses) and in the small signal electronic control (voltage regulator, current sensor, …) [6,28,29]. The proposed model allows the computation of the converter efficiency η_{DCDC}, knowing the power P_m applied to the electrical motor and the losses P_{losses} :

$$\eta_{DCDC} = \frac{P_m}{P_m + P_{losses}} \tag{3}$$

with

$$P_{losses} = P^c_{mosfet} + P^c_{diode} + P_{sw} + P^c_{ind} + P^{mag}_{ind} + P_{supply} \tag{4}$$

with P^c_{mosfet} and P^c_{diode} the conduction losses in the power components, P_{sw} the switching losses in the power stage, P_{supply} the control part consumption, P^c_{ind} and P^{mag}_{ind} the copper and magnetic losses in the smooth inductance.

Conduction losses in the Schottky diode and the power MOSFET can be easily calculated by considering an ideal waveform of the motor current i_m, has given by Fig. 4. Assuming a conduction time αT for the MOSFET, its

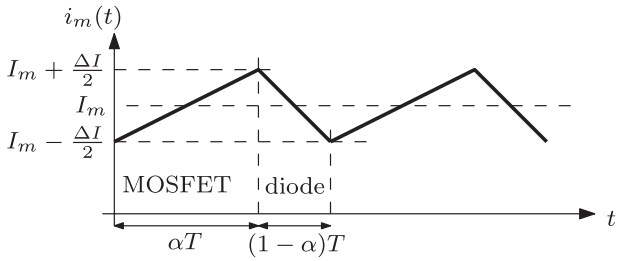

Fig. 4 – Ideal waveform of the DC-motor current i_m considered for losses calculation.

conduction losses for an average current I_m, with a current ripple ΔI, are given by:

$$P^c_{mosfet} = \frac{1}{T}\int_0^{\alpha T} R_{ds(on)}\, i_m^2(t)dt = R_{ds(on)}\,\alpha\left(\frac{\Delta I^2}{12} + I_m^2\right) \tag{5}$$

where $R_{ds(on)}$ is the equivalent resistance of the MOSFET and α the duty cycle, i.e. the ratio between the output voltage of the power stage and the voltage supplied by the fuel-cell. With the same approach, the conduction losses in the Schottky diode are given by:

$$\begin{aligned} P^c_{diode} &= \frac{1}{T}\int_{\alpha T}^{T} (U_{d0} + R_d i_m(t))\, i_m(t)dt \\ &= (1-\alpha)\left(R_d\frac{\Delta I^2}{12} + R_d I_m^2 + U_{d0} I_m\right) \end{aligned} \tag{6}$$

with U_{d0} the equivalent drop voltage of the diode and R_d its equivalent resistance.

For the switching losses in the power MOSFET and the Schottky diode, the considered waveforms are deliberately simplified and only allow a rough assessment of the switching losses. The used method for the MOSFET losses calculation is based on the gate charge characteristic [23,28–30]. The switch-on commutation starts once the gate voltage exceeds the threshold voltage $V_{gs(th)}$ (see Fig. 5). During fall-time of the MOSFET voltage (generally supposed greater than the current rise time which is generally neglected), the gate-to-source voltage V_{dr} is nearly constant due to the Miller effect. The gate current supplied by the driver is then given by:

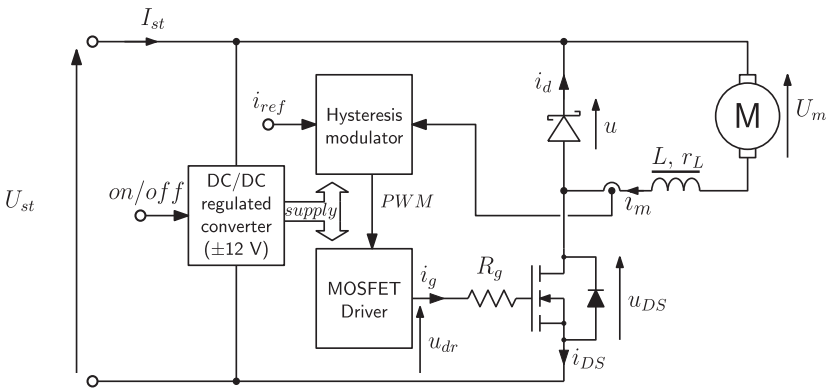

Fig. 3 – Diagram of the DC/DC power converter.

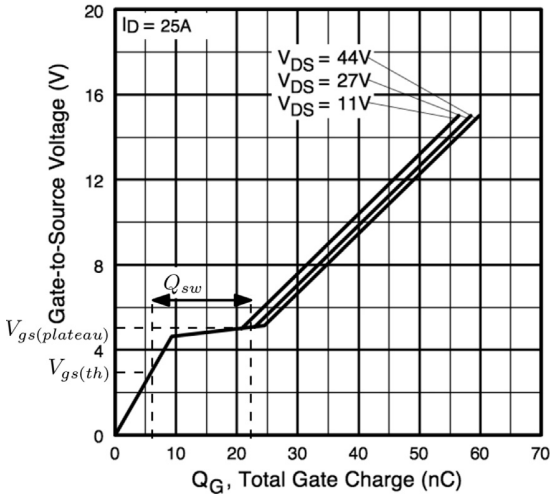

Fig. 5 – Total gate charge Q_{sw} during a commutation for the nominal current (from the IRFZ44N MOSFET datasheet).

$$I_g = \frac{V_{dr} - V_{gs(plateau)}}{R_g} \tag{7}$$

where R_g is the total gate resistance and $V_{gs(plateau)}$ is the value of the gate voltage during the switch-on transient, obtained from datasheet as illustrated by Fig. 5. The total gate charge Q_{sw} can also be deduced from this figure and finally, the switch-on time t_{on} can be obtained with:

$$t_{on} = \frac{Q_{sw}}{I_g} = R_g \frac{Q_{sw}}{V_{dr} - V_{gs(plateau)}} \tag{8}$$

The switch-off time t_{off} calculation is obtain from the same Eqs. (7) And (9), but this time with a null driver voltage V_dr:

$$t_{off} = R_g \frac{Q_{sw}}{V_{gs(plateau)}} \tag{9}$$

Now, the energy losses can be calculated, considering linear variations of the voltage and the current during the rise and fall times. At the switch-on time, the load current is equal to $I_m + \Delta I$. The switch-on energy is given by:

$$E_{on} = \frac{1}{2}(I_m + \Delta I) U_{st} t_{on} \tag{10}$$

At the switch-off time, the load current is equal to $I_m - \Delta I$ and the switch-off energy is then given by:

$$E_{on} = \frac{1}{2}(I_m - \Delta I) U_{st} t_{off} \tag{11}$$

Finally, the switching losses can be evaluated, knowing the switching frequency f_{sw}:

$$P_{sw} = (E_{on} + E_{off}) f_{sw} \tag{12}$$

For the coil inductance, used to smooth the current in the ironless motor, the losses occur in the aluminium winding (to reduce the weight of the coil) and in the iron core. With a current waveform as shown in Fig. 4 and with an equivalent serial resistance r_L, these losses are given by:

$$P_{ind}^{c} = \frac{1}{T}\int_0^T r_L i_m^2(t)dt = R_L\left(\frac{\Delta I^2}{12} + I_m^2\right) \tag{13}$$

For the core losses, hysteresis and eddy current have to be taken into account. But due to the high complexity to find analytical formulation, manufacturers typically used the Steinmetz relationship which only need three parameters and can be practically identified [26]. The conventional formulation of this relationship is obtained from the magnetic loss per unit, expressed in W/m^3 and given by:

$$p_{v\ mag} = k_m f_{sw}^{a} \Delta I^{b} \tag{14}$$

where k_m, a and b are parameters of the material. Knowing the core volume V_{core}, core losses are obtained by:

$$P_{ind}^{mag} = V_{core}\ p_{v\ mag} \tag{15}$$

Finally, the small signal electronic part consumption is taken into account by a constant power value P_{ctrl} and the Hall effect current sensor consumption P_{cs} is taken into account with a power proportional to the motor current I_m:

$$P_{supply} = P_{ctrl} + P_{cs} = k_{cs} V_{cs} |I_m| + P_{ctrl} \tag{16}$$

where V_{cs} is the supply voltage of the current sensor and k_{cs} the ratio between the measured current and the small signal current coming from the Hall-effect sensor.

Ironless DC-motor

The power converter supply a 200 W brushed DC motor with a nominal voltage of 24 V (MAXON RE50). The choice of this motor is linked to its high efficiency (above 94%) despite its low power rating. Moreover, the DC motor is iron-less, thus without hysteresis and eddy current losses. The losses in the DC motor are: the dry and viscous friction on the shaft, the Joule losses in the wiring and the voltages drop in the brushes. The expression of the motor efficiency can then be obtained from the following equation:

$$\eta_{motor} = \frac{k_\phi \omega_{mot}(I_m - (k_v\ \omega_{mot} + k_d))}{(k_\phi\ \omega_{mot} + r\ I_m + E_b) I_m} \tag{17}$$

where k_ϕ is the torque constant (Nm A^{-1}), ω_{mot} is the rotation speed (rad s^{-1}), I_m is the motor current (in A), k_v is the viscous friction constant (in A rad^{-1} s), k_d is the dry friction constant (in A), r is the wiring resistance (in Ω) and E_b is the voltage drop in the brushes (in V).

Mechanical modeling

In order to obtain the dynamical behavior of the vehicle, the mechanical equations must be solved. To run, the vehicle has to overcome the efforts due to the aerodynamic F_{aero}, the slope F_{slope} and the rolling resistance due to friction between the wheel and the road F_{rr}. The fundamental law of the mechanic gives the next equation to solve (see Fig. 6) [31]:

$$m\frac{dv(t)}{dt} = F_w - F_{rr} - F_{slope} - F_{aero} - F_{brake} \tag{18}$$

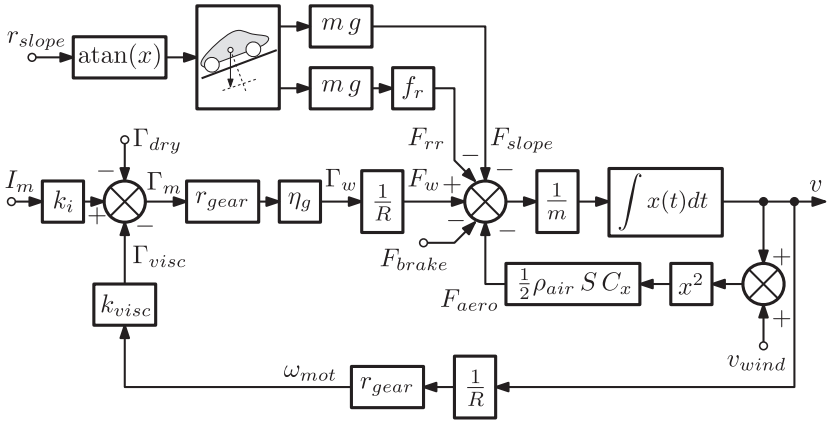

Fig. 6 – Dynamical model of the mechanical part of the vehicle.

where m is the mass of the vehicle, F_w is the propulsion force applied to wheel through the electrical motor and F_{brake} the mechanical braking force.

The aerodynamic force F_{aero} is computed from the mechanical parameters of the vehicle and the wind speed v_{wind} :

$$F_{aero} = \frac{1}{2}\rho_{air} S C_x (v(t) + v_{wind})^2 \tag{19}$$

with ρ_{air} the mass density of air, C_x the drag coefficient, S the frontal area, $v(t)$ and v_{wind} respectively the vehicle and wind velocities (in m s^{-1}). The forces due to the rolling resistance and the road inclination are calculated from the mass m of the vehicle and the slope r_{slope} given in %:

$$F_{rr} = m\, g\, f_r \cos(\arctan(r_{slope})) \tag{20}$$

$$F_{slope} = m\, g \sin(\arctan(r_{slope})) \tag{21}$$

The total drive Force F_w applied through both rear wheels is calculated from the motor torque Γ_m, such as:

$$F_w = \eta_g \frac{r_{gear}}{R} \Gamma_m \tag{22}$$

where R is the wheel radius, r_{gear} the gearbox ratio of the transmission and η_g its efficiency.

Thermal model of the fuel cell stack

The typical nominal power of a powertrain for an urban-concept car is below 1 kW. For such relatively low power need, the auxiliary devices of the system play a crucial role in the total energy consumption. It is well known that fuel cell stack auxiliaries cause a drop in system efficiency at low power. It is therefore necessary to take their consumption into account [3,4,7,15,16]. For this vehicle, the accessories of the fuel cell are limited to an air blower and a cooling fan. The operation and the consumption of these accessories are presented in this section. The thermal source $P_{th\ src}$ due to the irreversibilities of the electrochemical reaction, is removed through many different paths. In this work, it is considered that thermal removal is achieved by the air flow rate in fuel cell channels $P_{th\ ab}$, the liquid-vapor phase change $P_{th\ stm}$ of the water produced by the electrochemical reaction of the fuel cell, the natural convection $P_{th\ nat}$ and the forced convection assured by the cooling blower $P_{th\ cb}$. Thus, a dynamical thermal model can be expressed by next equation [19,20]:

$$m_{fc} C_p \frac{dT_{st}}{dt} = P_{th\ src} - P_{th\ ab} - P_{th\ stm} - P_{th\ nat} - P_{th\ cb} \tag{23}$$

The thermal source $P_{th\ src}$ is calculated from the total power supplied by the PEMFC and its polarization curve:

$$P_{th\ src} = (n_{cells}\, E_{Nernst} - U_{st}) I_{st} \tag{24}$$

where E_{Nernst} is the reversible voltage of a cell, calculated from the Nernst equation [22,25] and n_{cells} the number of cells.

The air flow in the air channel, produced by the air blower, permits to remove a part of the heat by forced convection. The air flow $Q_{v\ ab}$ (in $l\ min^{-1}$), for given Stoechiometric-ratio S_c and stack current I_{st}, is given by next equation:

$$Q_{v\ ab} = 60000 \frac{5 R_c (273,15 + T_{st})}{4 P_a f} I_{st} n_{cells} S_c \tag{25}$$

with R_c the ideal gas constant (8.31 J mol^{-1} K^{-1}, T_{st}) the stack temperature (in °C) and P_a the atmospheric pressure (101,300 Pa). By assuming a perfect exchange between the air channel and the stack, the output of air temperature is equal to the mean stack temperature (T_{st}). Moreover, the input air temperature is equal to the ambient T_{amb}. Then the evacuated thermal power is:

$$P_{th\ ab} = \frac{1}{60} \rho_{air} Q_{vair} C_{pair} (T_{st} - T_{amb}) \tag{26}$$

where ρ_{air} is the air density (1.2 kg m^{-3}), C_{pair} its specific heat (1000 J K^{-1} kg^{-1}).

The transport of water through the different fuel cell components (membrane, diffusion layers and channels) is still being debated by the scientific community. However, with the emergence of imaging techniques, such as X-ray or Neutron radiography, the co-existence of vapor and liquid water within the fuel cell has been emphasized by several authors [2,9,13,14,21]. In presence of saturated gas in cathode channels, the water produced in vapor at the catalyst layer flows through the microporous layer before to condensate in the

macro-porous layer. The liquid water is then transported under capillary fingering regime and removed toward the channels in an eruptive regime [14,21]. Nevertheless, the particular fuel cell operating conditions used in this study, i.e. low current density, high air stoichiometry, low relative humidity (ambient air) and dead-ended anode, may lead to significantly different transport regime. As a result, Lee et al. [18] reported an absence of liquid water in the channels of a fuel cell operating in similar conditions. According to this, the present model assumed that the liquid water presents in the GDL is evaporated and drained through the channel in vapor form. Thus, the power drained by the liquid-vapor phase change is given by:

$$P_{th\ stm} = \dot{m}_{H_2O} L_{H_2O} \tag{27}$$

where $\dot{m}_{H_2O}$ is the water mass flow-rate (g s^{-1}) evacuated through the air channel and L_{H2O} the latent heat of vaporization (2500 kJ kg^{-1}). The amount of water produced by the reaction depends only on the stack current I_{st} provided by the fuel cell. The flow-rate $\dot{m}_{H_2O}$ is then given by the following equation:

$$\dot{m}_{H_2O} = n_{cells} \frac{R_c (273.15 + T_{st})}{4 P_a F} I_{st} \tag{28}$$

The natural convection exchange coefficient is deduced from experimental measurements and expressed as:

$$P_{th\ nat} = k_{nat} (T_{st} - T_{amb}) \tag{29}$$

The last term of Eq. (23) is the forced convection by the cooling blower. For the studied fuel cell stack, each cell is separated from the other by a corrugated iron sheet. Knowing the air flow-rate $\dot{m}_{cb}$ (attention, $Q_{v\ cb}$ après) and considering a perfect exchange with the fuel cell, the thermal power removed by the cooling blower is given by:

$$P_{th\ cb} = \rho_{air} Q_{v\ cb} C_{p\ air} (T_{st} - T_{amb}) \tag{30}$$

Now that each part of the thermal model was described, its coupling with the electrical model of the fuel cell stack and accessories must be done. From the stack current I_{st} and temperature T_{st}, Eq. (26), (27) and (29) can be directly calculated. For Eq. (30), the air flow rate is an input parameter for the model. In this work, it is considered that the cooling blower is controlled through its voltage U_{cb}. The same assumption is made for the control of the air blower (U_{ab}).

The air flow rate of the cooling blower and air feeding fan are measured on a fuel-cell stack made of 28 cells (31 cm^2 of active area) manufactured by the society *MES* [24]. The cooling system is a 12 V radial blower, Micronel U97 and the air feeding fan is a 12 V axial blower, Micronel D484.

Measurements on this fuel cell assembly allow to deduce the airflow and power consumption of the auxiliaries, as shown in Fig. 7.

For both blower, a least squares regression is used to fit the experimental datas:

$$Q_{v\ ab} = 0.75 U_{ab} \text{ and } P_{ab} = 4.0 U_{ab}^3 \tag{31}$$

$$Q_{v\ cb} = 4.00 U_{cb} \text{ and } P_{cb} = 7.5 U_{cb}^3 \tag{32}$$

Driving and auxiliary management laws

The last part of the model to be detailed is the supervision with the control laws. These functions are performed by a microcontroller ATMEGA 128. This system receives and processes various information such as the setting motor current, stack temperature, fuel cell current, vehicle velocity, etc.

For the cooling regulation, an hysteresis controller is used. The cooling blower is turned on with a given voltage value, if the temperature exceed a threshold value T_{max} and while it remains greater than a lower value T_{min}. Even if this control law is not optimal, it has the advantage of being extremely robust with respect to changes in operating conditions (stack losses, ambient temperature, …). Further, to smooth the power supplied by the stack, the cooling blower is supplied only during the free-wheel phase (i.e. deceleration phase), when the electrical motor is turned off and the vehicle consumption is minimum (see Fig. 8).

For the driving strategy, each lap of the race can be decomposed in three sequences. The first one is a starting phase from 0 km/h to an intermediate velocity v_{min}, with a constant motor current I_{start}. During this phase, the acceleration should be high enough so as not to lose too much time for the rest of the lap. In contrast, for a too high torque applied to the wheel, the power train efficiency could be greatly reduced.

The second phase is a *constant speed* strategy. The objective is to maintain an average speed as constant as possible, with the greatest possible efficiency. In Ref. [34], it is shown that the optimum efficiency is obtained by performing a series of acceleration and free wheel. The acceleration phases are carried out with the optimum torque, which maximizing the energy efficiency of the power chain. The parameters to be optimized are the motor current I_{acc} applied during the acceleration phases and speed hysteresis thresholds v_{min} and v_{max}. The optimization of these parameters must improve the global energetic performance of the vehicle.

Formulation of the optimization problem

For the optimization of this problem, a standard formulation is used. The objective function can be expressed has *the minimization of the fuel consumption on a full race (10 laps), under constraint of a minimum average speed of 25 km/h*. The tank-to-wheel model illustrated by Fig. 2 is implemented in Matlab. The state-space variables taken into account are the fuel consumption m_{H2}, the velocity $v(t)$ and the stack temperature $T_{st(t)}$, according to Eqs. (18) and (23). Both equations are computed using a 4th order Runge-Kutta solver for one lap and using a relaxation method to reach a thermal equilibrium. Indeed, it is easier and safer to rely on a nominal thermal operating point. The problem is then formulated as an ordinary differential equation (ODE) such as:

$$\frac{dx}{dt} = f(x,t), \text{ with } x(0) = x_0 \tag{33}$$

where the state space vector $x(t) = [v,\ T_{st},\ m_{H2}]^T$. The relaxation method intends to reinject the final temperature value of the simulation (one lap here) as the initial value of the next calculation. To accelerate the convergence, the initial temperature is chosen equal to the lower bound of the

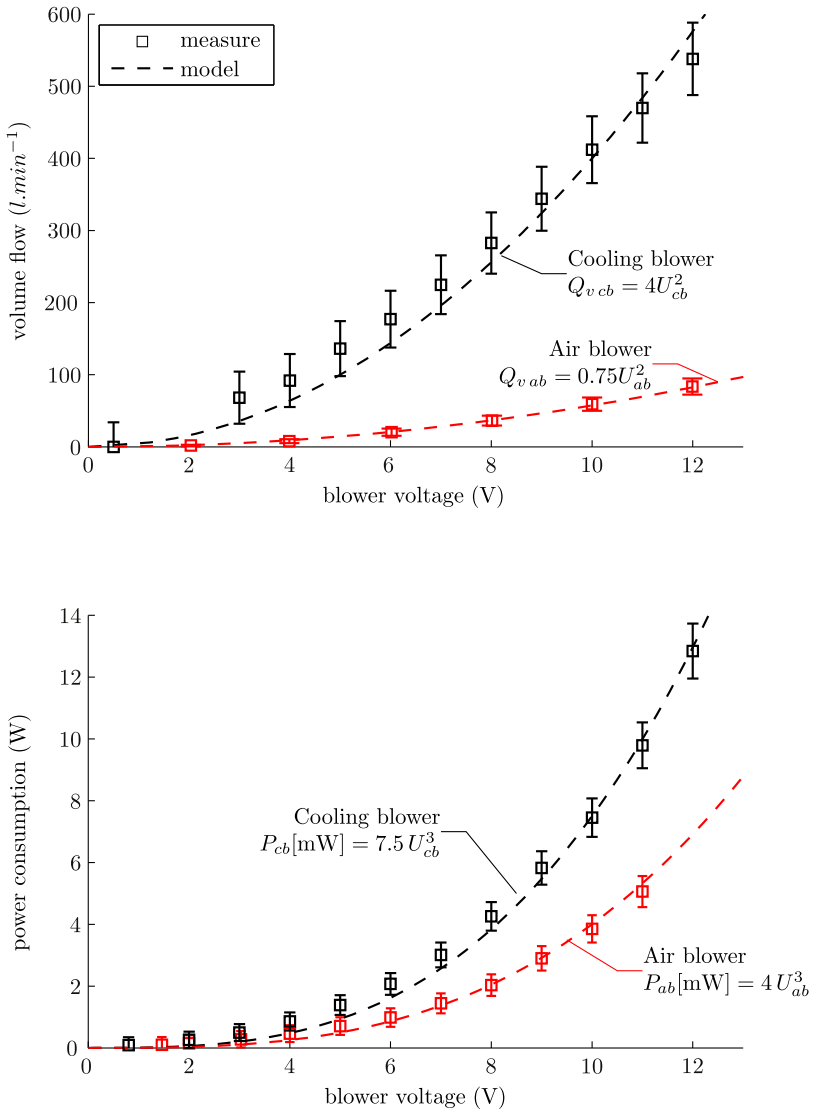

Fig. 7 – Characteristics of the cooling and air blowers.

regulator (around 40 °C). The steady state is achieved in just a few iterations.

For the optimization, a particle swarm algorithm is used with five input parameters (see Fig. 8), which are the motor currents I_{start} and I_{acc}, the maximum speed v_{max}, the speed ripple ΔV which is the difference between v_{max} and v_{min}, and the gearbox ratio r_{gear} between the electric motor and the wheel. The tuning of the particle swarm algorithm is classical, with a population of 50 particles and a maximum number of iterations of 200 [12]. To sum up, the optimization problem can be formulated such as:

Minimize: $g(\mathbf{p}) = (\text{fuel consumption})$

with: $\mathbf{p} = \{I_{start}; I_{acc}; v_{max}; \Delta V; r_{gear}\}$

subject to: $\text{mean}(v(t)) \geq 25\text{km/h}$ and $\max(T_{st}(t)) < 45^{\circ}\text{C}$

Both constraints are evaluated at the end of each simulation. If a constraint is not respected, the solution is degraded by the addition of a weight on the objective function:

$$g(\mathbf{p}) \leftarrow g(\mathbf{p}) + 2^{\frac{25-\text{mean}(v)}{f_v}} + 2^{\frac{\max(T_{st})-45}{f_T}} \quad (34)$$

where f_v and f_T are the setting weights on the velocity and temperatures respectively.

Results

The optimization results for the runs of the shell eco marathon in Rotterdam is summarized by Table 1. This optimization takes into account the slope of the road and is obtained for an ambient temperature of 25°C. The list of the vehicle parameters, used for the optimization, is given by Table 3. As shown in Fig. 9, the vehicle is launch in 30 secondes (0–25 km/

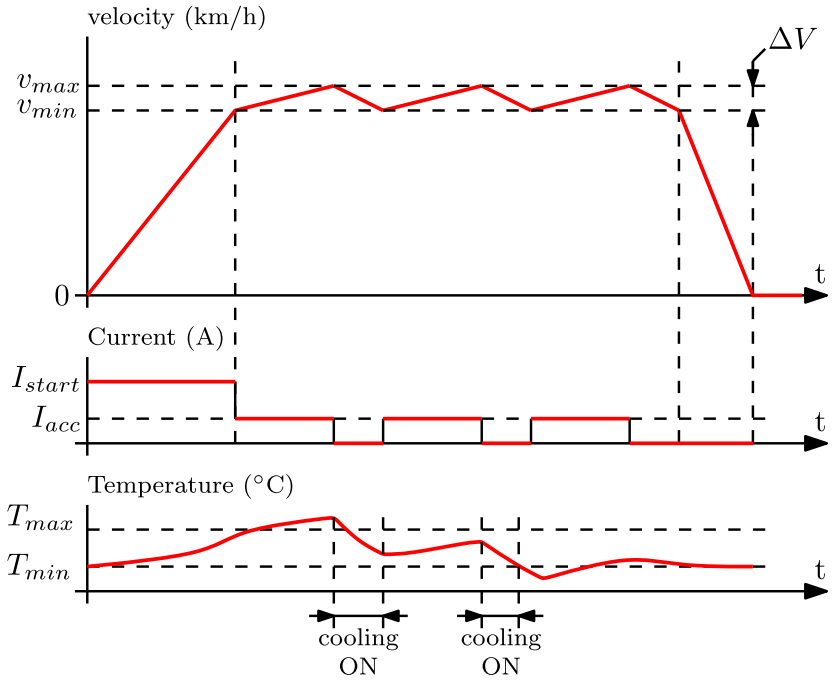

Fig. 8 – Typical speed, current and temperature profiles for each lap.

Table 1 – Optimization result.

Parameter	Value
I_{start}	10.8 A
I_{acc}	3.1 A
v_{max}	27.8 km/h
ΔV	1.6 km/h
r_{gear}	200/14
Average velocity	25.0 km/h
Fuel cell losses	3.04 Wh/lap
Motor losses	0.39 Wh/lap
DC-DC converter losses	0.23 Wh/lap
Mechanical transmission losses	0.11 Wh/lap
Supervision system consumption	0.37 Wh/lap
Mechanical energy	3.7 Wh/lap
Hydrogen consumption	7.96 Wh/lap
Tank-to-wheel efficiency	46.20%
Performance	4.94 Wh/km
	1855.75 km/L_{SP95}

Table 3 – Parameters of the vehicle.

Parameter	Symbol	Value
mass	M	150 kg
drag coefficient	C_x	0.1
frontal area	S	0.88 m^2
air density	ρ_{air}	1.2 kg m^{-3}
rolling resistance coefficient	f_r	2.10^{-3}
transmission efficiency	η_g	0.95
number of cells	n_{cells}	28
mass of the fuel cell	m_{fc}	1 kg
heat capacity of the fuel cell	C_p	750 J kg^{-1} K^{-1}
heat capacity of the air	$C_{p\,air}$	1000 J kg^{-1} K^{-1}
latent heat of vaporization	L_{H_2O}	2500 kJ kg^{-1}
natural convection coefficient	k_{nat}	0.25 W K^{-1}
ambiant temperature	T_{amb}	25°C
high threshold temperature	T_{max}	44°C
low threshold temperature	T_{min}	41°C
oxygen stoechiometric-ratio	S_c	5

Table 2 – Sensitivity of the optimization results against parameter variations.

	Reference	I_{start}	I_{acc}	v_{max}	ΔV	r_{gear}
optimization		10.8 A	3.1 A	27.8 km/h	1.6 km/h	200/14
variations		+0.1 A	+0.1 A	+1.0 km/h	+0.1 km/h	–
consumption	4.9 Wh/km	+0.90%	+0.08%	+2.59%	+3.14%	–
average speed	25.0 km/h	+0.21%	+0.04%	+1.23%	+0.18%	–
Stack temperature	42.90C◦	+0.05%	+0.02%	+0.32%	+0.15%	–

h). An average speed of 27 km/h is then maintained with a small velocity ripple of ΔV = 1.6 km/h, due to the successions of acceleration and free wheel phases. At the end the vehicle is able to brake very quickly and efficiently. During the lap, and by considering an initial temperature of 41°C, the cooling system is activated during the free wheel phases to maintain a stack temperature between 41 and 44°C.

With this set of parameters, the global tank-to-wheel efficiency for one lap of the race is greater than 45% and an energy performance of about 500 Wh/100 km (i.e. an equivalent

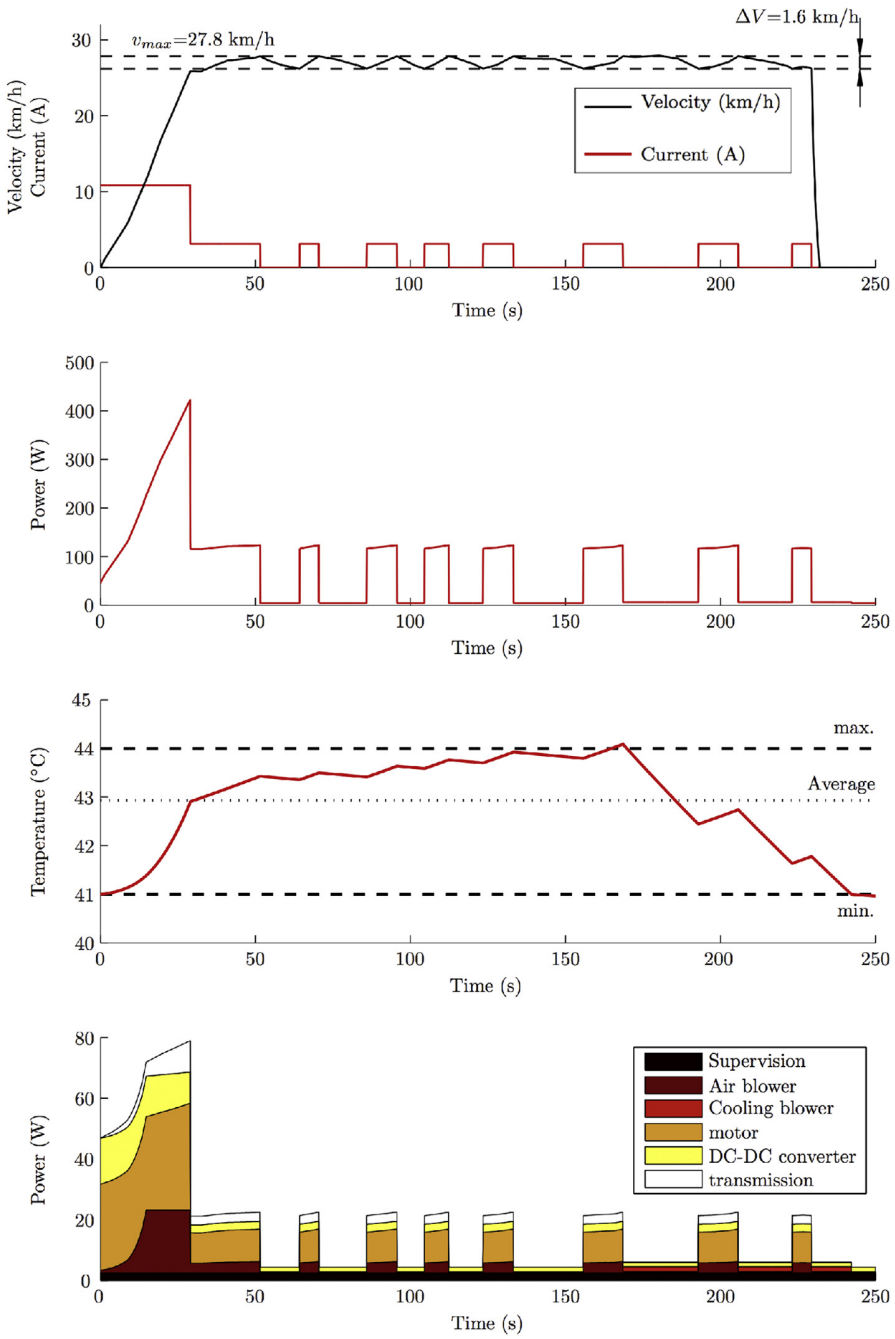

Fig. 9 – Optimal profiles for one lap of the Cityjoule vehicle, on the Rotterdam race.

consumption of 1 L_{SP95} for 1800 km) is achieved. This simulation result is obtained for ideal climatic conditions without wind. This performance can thus be viewed as being the maximum value to be reached by the vehicle.

Considering the thermal behavior of the fuel cell, the proposed dynamical model permits to estimate the repartition of the heat through the various possible paths (natural convection, air feeding, liquid to vapor phase, cooling system). Fig. 10 gives the thermal power repartition in steady state, to maintain an average temperature of 43°C, as shown on Fig. 9. Heat is thus mainly evacuated by the cooling system and the liquid to steam phase change of the water produced by the reaction. It must be noted that the assumption of a complete conversion to steam of the water produced in liquid form is still debated by the scientific community [14,17,18,21]. That is why in future works, experimental measurements must be done to confirm this hypothesis.

Fig. 11 presents the Sankey diagram of the powertrain for a lap. This energy diagram reveals that the main source of energy loss is the PEMFC stack: 38% of the primary hydrogen

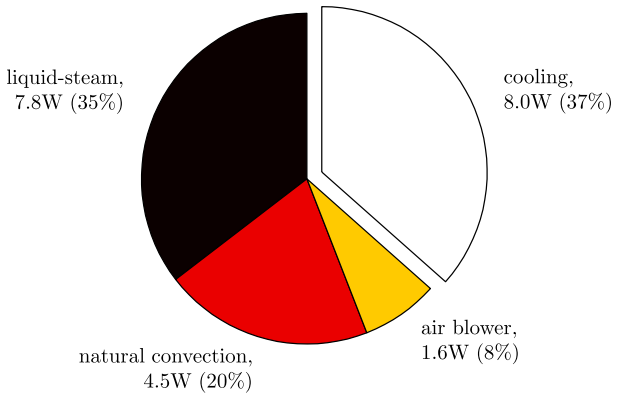

Fig. 10 – Heat evacuation paths for an average temperature of 43°C.

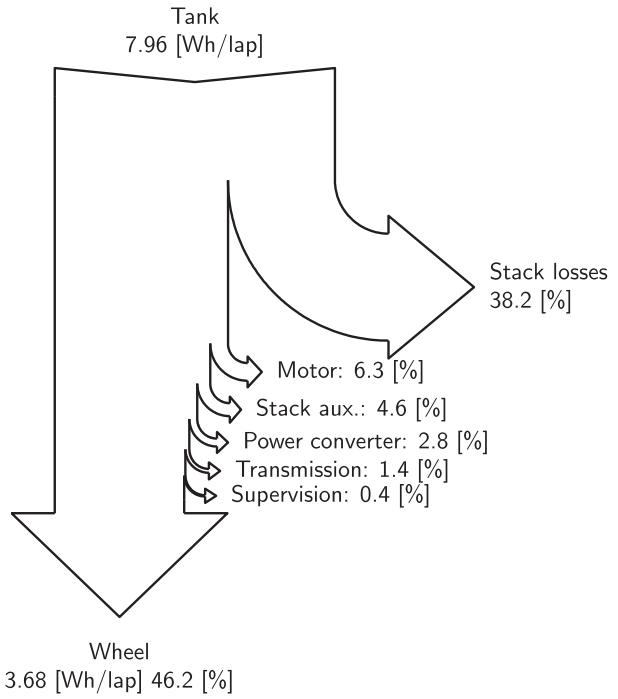

Fig. 11 – Sankey diagram for one lap.

energy is lost in the electrochemical process. A total of 4.6% of the primary energy is consumed by the fuel cell stack auxiliaries, constituted by the air blower and the cooling fan. Finally, 46% of the primary hydrogen energy is available to the wheel.

Finally, a sensitivity analysis is conducted on the optimization results (see Table 2). From the data set obtained by optimization, each variable is slightly modified to assess its influence on different criteria. Thus, the starting current and the acceleration current are increased by 0.1 A, the maximum speed by 1 km/h and the speed ripple by 0.1 km/h. Because the gear ratio is not considered as a strategy variable, it is not modified. The sensitivity is computed on 3 different parameters, which are the performance, the average speed and the average value of the stack temperature along 1 lap.

These results show that the sensitivity of the driving strategy on the performance is quite high and especially on the velocity profile v_{max} and ΔV. A variation of only 1 km/h on the maximum speed lead to a consumption increase of more than 2%. This sensitivity is mainly due to the higher aerodynamic drag when the velocity increases. A quite high sensitivity on the performance is also obtained for the starting and acceleration currents, which is due this time to a global lower efficiency of the powertrain. An important criterion of a race is to consider the minimum average speed of 25 km/h. It is interesting to see that the increase in the motor current (i.e. torque) does not significantly increase the average speed vehicle, while it increases the vehicle consumption. It seems then more interesting to increase the maximum speed, while keeping the same velocity ripple and motor current. With this strategy, the powertrain efficiency remains optimum, as well as the average number of starts per lap. Finally, a sensitivity analysis is done on the average stack Temperature, which is representative of the mean value of the stack losses. Once again, the higher sensitivity is on the velocity profile, due to an higher mechanical need when the average speed increase. As a conclusion, the velocity ripple, starting current and acceleration current must be as close as there values obtained by optimization. To adapt the speed of the car during a race, only the maximum velocity has to be changed.

Experimental results on the Rotterdam track

During the 2015 edition of the Shell Eco-marathon, which took place in May in the city center of Rotterdam, Netherlands, a full run has been recorded. The measurements include the instantaneous speed (via an in-vehicle GPS), the voltage and current of both fuel cell stacks, and the stack temperature (through a PT1000 sensor). The total distance covered is of 16 km which is performed in 10 laps. With an average speed of 25 km/h, the duration of a run must not be more than 38 min (i.e. 2300 s). Fig. 12 gives a comparison between experimental results and simulation results obtained in the same conditions, ie an ambiant temperature of 27°C (which is the temperature inside the fuel cell compartment) and an equivalent average wind speed of 15 km/h.

Finally, the measured results are very close to simulations. The power supplied by each fuel cell stack reached in both cases up to 250 W, as well as the average power which is about 110 W. As explain before, the driving strategy bases on changing only the maximum speed during the race, to adapt the average speed per lap. Concerning the stack temperature, the low and high thresholds are 5°C higher than in the previous section of this paper. This is due to the fact that the temperature measurement is placed at the hottest point, which is about 4–5°C above the average stack temperature. With this slight adjustment, a good agreement is obtained. The recorded performance for this run is 796 Wh/100 km, by considering a lower heating value of 33 kWh/kg and a volumic density of 0.08988 kg m^{-3}. The simulation results give a consumption of 820 Wh/100 km, that is to say an error of only 3%. The difference with the performance of 500 Wh/100 km obtained with ideal climatic conditions (see the previous section)

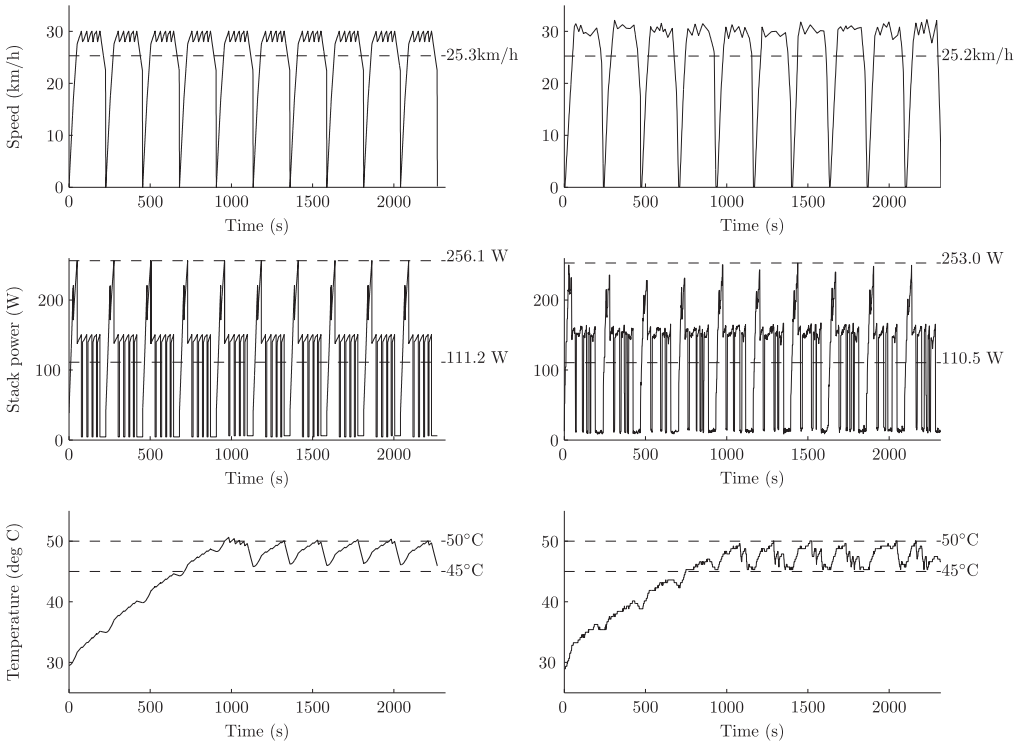

Fig. 12 – Experimental (left) and simulation (right) results of a race on the Rotterdam track during the Shell Eco-Marathon 2015.

and this measured result is mainly explained by the meteorological conditions, and especially wind.

Conclusions

In this paper, an analytical tank-to-wheel model of an Urban-Concept fuel cell vehicle is presented. It takes into account the mechanical needs, the losses of each stage of the power train (fuel cell and auxiliaries, power converter, motor, transmission) and the dynamical thermal behavior of the fuel cell to account accurately the consumption of the fuel cell stack auxiliaries. Using a set of five driving parameters (speed thresholds, gear ratio and motor currents), an optimal driving strategy is obtained using a global optimization algorithm. This multiphysical and dynamic model is based on the consumption and the main interactions between the various elements of the car. Therefore, the optimal driving strategy is obtained using a global optimization algorithm which accounts for race constraints. This optimization leads to a maximum performance of 500 Wh/100 km for this urban vehicle, with an average speed of 25 km/h. A sensitivity analysis is done and shows that to adjust the average speed of the vehicle during a real race, it is recommended to change the maximum value of the speed profile without changing the motor currents or the velocity ripple. Today, the powertrain of this urban concept vehicle does not includes storage elements for the braking energy recovering. This is mainly explained by the ultra lightweight of the vehicle. Indeed, with a total weight of 150 kg, the total recoverable kinetic energy at 25 km/h is only 1 Wh. Since each lap requires about 8 Wh of hydrogen energy, the potential gain from such an energy recovery system remains below than 15%. Nevertheless, in the context of such energy competitions, any gain of consumption is valuable. This is why the integration of supercapacitors in the vehicle is planed.

Acknowledgment

The research leading to these results has received funding from the European Union's Seventh Framework Programme (FP7/2007-2013) under grant agreement ETRERA 2020 num. [609543].

REFERENCES

[1] Ettihir Khalid, Boulon Loic, Agbossou Kodjo. Energy management strategy for a fuel cell hybrid vehicle based on maximum efficiency and maximum power identification. IET Electr Syst Transp December 2016;6(4):261–8.

[2] Antonacci P, Chevalier S, Lee J, Yip R, Ge N, Bazylak A. Feasibility of combining electrochemical impedance spectroscopy and synchrotron x-ray radiography for determining the influence of liquid water on polymer electrolyte membrane fuel cell performance. Int J Hydrogen Energy 2015;40(46):16494–502. http://www.sciencedirect.com/science/article/pii/S0360319915300562.

[3] Bao C, Ouyang M, Yi B. Modeling and optimization of the air system in polymer exchange membrane fuel cell systems. J Power Sources 2006;156(2):232–43.
[4] Boulon L, Agbossou K, Hissel D, Sicard P, Bouscayrol A, Péra M-C. A macroscopic pem fuel cell model including water phenomena for vehicle simulation. Renew energy 2012;46:81–91.
[5] Boulon L, Hissel D, Bouscayrol A, Pera M-C, Delarue P. Multi physics modelling and representation of power and energy sources for hybrid electric vehicles. In: Vehicle power and propulsion conference, 2008. VPPC'08. IEEE. IEEE; 2008. p. 1–6.
[6] Brik K, Ammar FB. Improved performance and energy management strategy for proton exchange membrane fuel cell/backup battery in power electronic systems. Int J Hydrogen Energy 2017;42(13):8845–56. http://www.sciencedirect.com/science/article/pii/S0360319916316482.
[7] Brodrick C-J, Lipman TE, Farshchi M, Lutsey NP, Dwyer HA, Sperling D, et al. Evaluation of fuel cell auxiliary power units for heavy-duty diesel trucks. Transp Res Part D Transp Environ 2002;7(4):303–15.
[8] Chevalier S, Auvity B, Olivier J-C, Josset C, Trichet D, Machmoum M. Detection of cells state-of-health in pem fuel cell stack using EIS measurements coupled with multiphysics modeling. Fuel Cells 2014;14(3):416–29.
[9] Chevalier S, Lee J, Ge N, Yip R, Antonacci P, Tabuchi Y, et al. In operando measurements of liquid water saturation distributions and effective diffusivities of polymer electrolyte membrane fuel cell gas diffusion layers. Electrochim Acta 2016;210:792–803.
[10] Chevalier S, Trichet D, Auvity B, Olivier J-CO, Josset C, Machmoum M. Multiphysics DC and AC models of a pemfc for the detection of degraded cell parameters. Int J Hydrogen Energy 2013;38(26):11609–18. http://www.sciencedirect.com/science/article/pii/S0360319913009506.
[11] de Miranda P, Carreira E, Icardi U, Nunes G. Brazilian hybrid electric-hydrogen fuel cell bus: improved on-board energy management system. Int J Hydrogen Energy 2017;42(19):13949–59. special Issue on the 21st World Hydrogen Energy Conference (WHEC 2016), 13-16 June 2016, Zaragoza, Spain, http://www.sciencedirect.com/science/article/pii/S0360319917300216.
[12] Eberhart RC, Kennedy J. A new optimizer using particle swarm theory. In: Proceedings of the sixth international symposium on micro machine and human science, vol. 1; 1995. p. 39–43. New York, NY.
[13] Ge N, Chevalier S, Lee J, Yip R, Banerjee R, George MG, et al. Non-isothermal two-phase transport in a polymer electrolyte membrane fuel cell with crack-free microporous layers. Int J Heat Mass Transf 2017;107:418–31. http://www.sciencedirect.com/science/article/pii/S001793101630730X.
[14] Hartnig C, Manke I, Kuhn R, Kardjilov N, Banhart J, Lehnert W. Cross-sectional insight in the water evolution and transport in polymer electrolyte fuel cells. Appl Phys Lett 2008;92(13):134106.
[15] Kandlikar SG, Lu Z. Thermal management issues in a pemfc stack–a brief review of current status. Appl Therm Eng 2009;29(7):1276–80.
[16] Lebreton C, Damour C, Benne M, Grondin-Perez B, Chabriat J-P. Passive fault tolerant control of {PEMFC} air feeding system. Int J Hydrogen Energy 2016;41(34):15615–21. http://www.sciencedirect.com/science/article/pii/S0360319916304153.
[17] Lee J, Hinebaugh J, Bazylak A. Synchrotron x-ray radiographic investigations of liquid water transport behavior in a pemfc with mpl-coated gdls. J Power Sources 2013;227:123–30.
[18] Lee Y, Kim B, Kim Y. An experimental study on water transport through the membrane of a pefc operating in the dead-end mode. Int J hydrogen energy 2009;34(18):7768–79.
[19] Li X, Deng Z-H, Wei D, Xu C-S, Cao G-Y. Parameter optimization of thermal-model-oriented control law for pem fuel cell stack via novel genetic algorithm. Energy Convers Manag 2011a;52(11):3290–300.
[20] Li Y, Xu S, Yang Z, Li Y. Control strategy and thermal management system research of fuel cell engine in sub-freezing. In: Mechanic automation and control engineering (MACE), 2011 second international conference on. IEEE; 2011b. p. 4830–3.
[21] Manke I, Hartnig C, Grünerbel M, Lehnert W, Kardjilov N, Haibel A, et al. Investigation of water evolution and transport in fuel cells with high resolution synchrotron x-ray radiography. Appl Phys Lett 2007;90(17):174105.
[22] Mann RF, Amphlett JC, Hooper MA, Jensen HM, Peppley BA, Roberge PR. Development and application of a generalised steady-state electrochemical model for a pem fuel cell. J Power Sources 2000;86(1):173–80.
[23] Melito M, Belverde G. Stripfet™ III and optimal choice of MOSFETs in high current VRMs. STMicroelectronics, Application Note AN1730. 2003.
[24] MES 05. Fuel cell manufacturer. 2017. http://www.cebi.com.
[25] Nguyen TV, White RE. A water and heat management model for proton-exchange-membrane fuel cells. J Electrochem Soc 1993;140(8):2178–86.
[26] Oliver C. A new core loss model. Switch Power Mag 2002;3(2):28–30.
[27] Olivier J-C, Bernard N, Bourguet S, Aranguren LM. Techno-economic optimization of flywheel storage system in transportation. In: Symposium de Génie Électrique 2014; 2013.
[28] Olivier J-C, Wasselynck G, Trichet D, Auvity B, Josset C, Le-Bozec C, et al. Power source to wheel model of a high efficiency fuel cell based vehicle. In: Vehicle power and propulsion conference (VPPC), 2010 IEEE; Sept 2010. p. 1–6.
[29] Olivier J-C, Wasselynck G, Trichet D, Auvity B, Josset C, Maindru P, et al. Light-duty fuel-cell vehicle designed for energetic races: high efficiency power converter design. Eur J Electr Eng 2012;15(1):39–61.
[30] Sodhi R, Kinzer D. Integrated design environment for dc/dc converter fet optimization. In: Power semiconductor devices and ICs, 1999. ISPSD'99. Proceedings, the 11th international symposium on. IEEE; 1999. p. 241–4.
[31] Souffran G, Miègeville L, Guérin P. Simulation of real-world vehicle missions using a stochastic markov model for optimal powertrain sizing. Veh Technol IEEE Trans 2012;61(8):3454–65.
[32] Squadrito G, Andaloro L, Ferraro M, Antonucci V. Hydrogen fuel cells technology. In: Basile A, Iulianelli A, editors. Advances in Hydrogen Production, storage and distribution. Woodhead Publishing Limited, Ch. 16; 2014.
[33] Thounthong P, Rael S, Davat B. Energy management of fuel cell/battery/supercapacitor hybrid power source for vehicle applications. J Power Sources 2009;193(1):376–85.
[34] Trichet D, Chevalier S, Wasselynck G, Olivier J-C, Auvity B, Josset C, et al. Global energy optimization of a light-duty fuel-cell vehicle. In: Vehicle power and propulsion conference (VPPC), 2011 IEEE. IEEE; 2011. p. 1–6.
[35] Trieste S, Hmam S, Olivier J-C, Bourguet S, Loron L. Techno-economic optimization of a supercapacitor-based energy storage unit chain: application on the first quick charge plug-in ferry. Appl Energy 2015;153(0):3–14. supercapacitors, http://www.sciencedirect.com/science/article/pii/S0306261915005164.
[36] Uherek E, Halenka T, Borken-Kleefeld J, Balkanski Y, Berntsen T, Borrego C, et al. Transport impacts on atmosphere and climate: land transport. Atmos Environ 2010;44(37):4772–816.

[37] Veziroglu A, Macario R. Fuel cell vehicles: state of the art with economic and environmental concerns. Int J Hydrogen Energy 2011;36(1):25–43.
[38] von Helmolt R, Eberle U. Fuel cell vehicles: status 2007. J Power Sources 2007;165(2):833–43.
[39] Wasselynck G, Auvity B, Olivier J-C, Trichet D, Josset C, Maindru P. Design and testing of a fuel cell powertrain with energy constraints. Energy 2012;38(1):414–24.